BARYONIC ACOUSTIC OSCILLATIONS

The clustering of matter encodes a preferred scale, the sound horizon at the baryon drag epoch of the early universe. This feature, which is imprinted on the matter distribution of the early universe by physics around recombination and earlier, is stretched with the expansion of the universe, appearing at a comoving galaxy separation of r_d ~ 150 Mpc. Since galaxies trace the matter content of the universe, the BAO feature is transferred into galaxy clustering, where it manifests as a single localised peak in the galaxy correlation function and an oscillatory signature, or "wiggles", in the galaxy power spectrum. The signature is also visible in other tracers of mass such as fluctuations in the Lyman-α forest — spectral features that indicate the radial distribution of neutral hydrogen clouds between the observer and distant quasars, as well as the CMB. Using BAO we can test for dark energy dynamics and spatial curvature, and in combination with other probes constrain the Hubble constant, the sum of neutrino masses, and the number of light species.

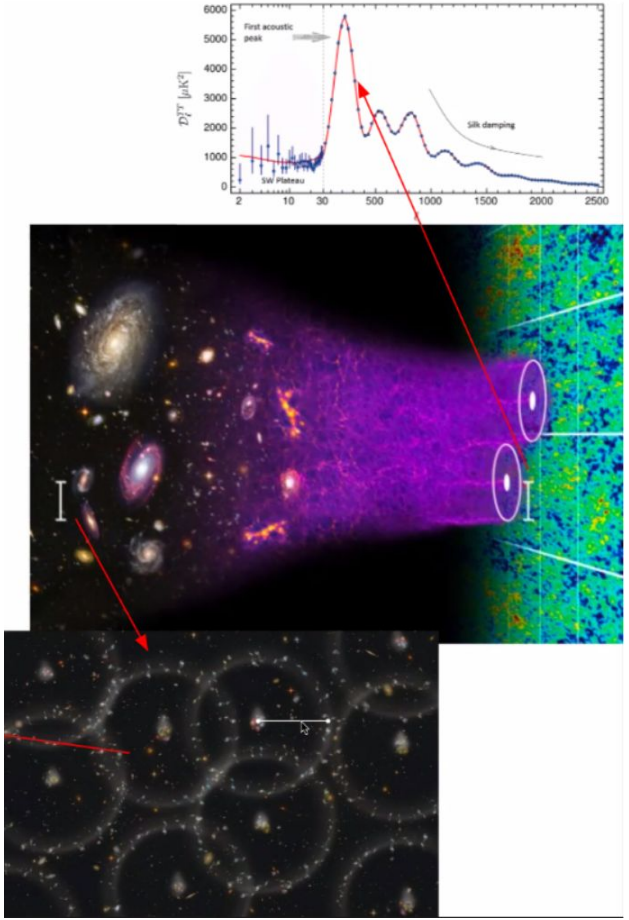

BARYONIC ACOUSTIC OSCILLATIONS

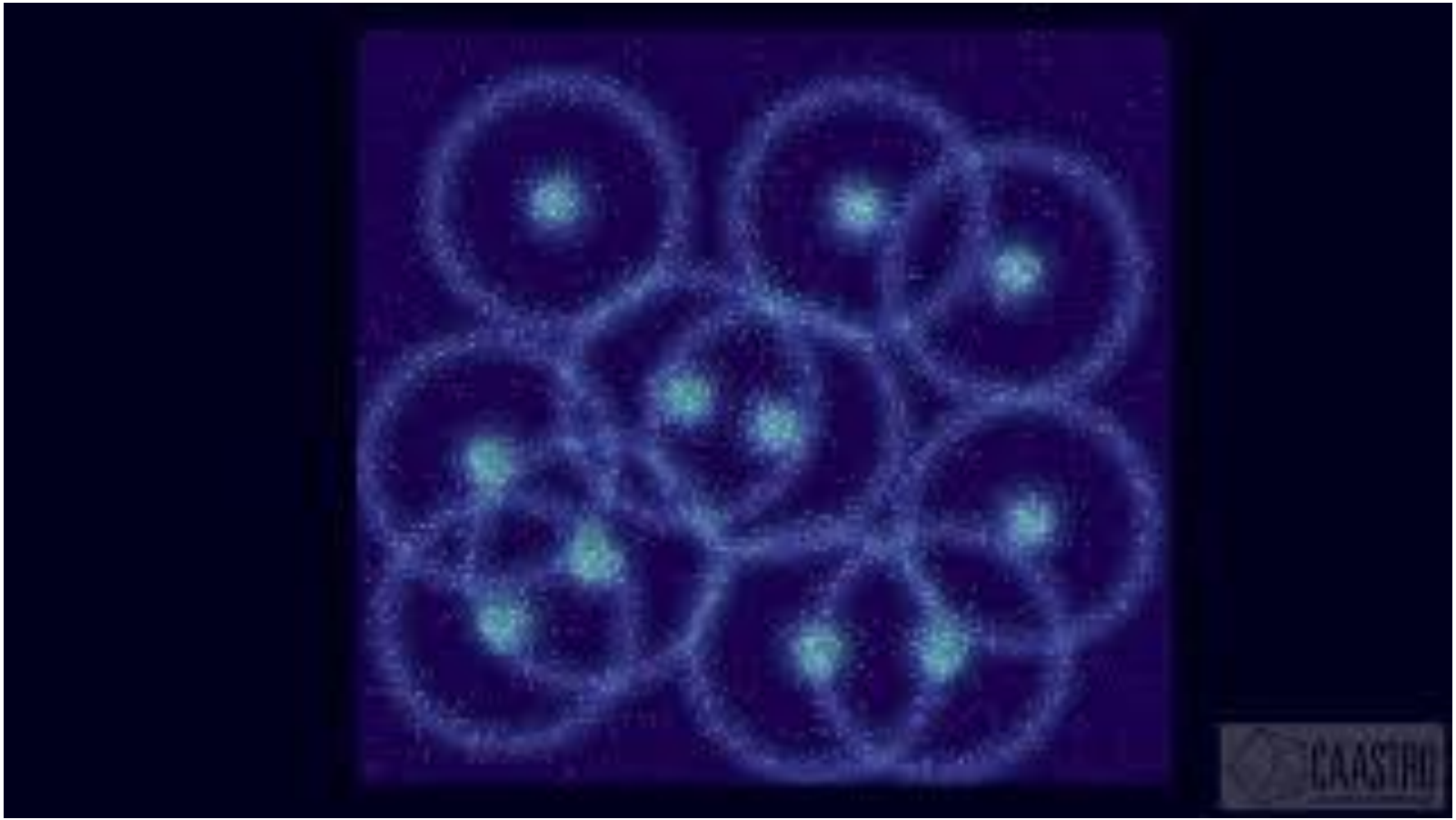

BAO AS STANDARD RULER

The physics of the propagation of the baryon waves in the early universe is fairly simple, and the sound horizon at drag epoch (~recombination) can be predicted, making r_d is a standard ruler. The (comoving) distance that sound can travel before the drag epoch (which indicates the time when the baryons decoupled (at $z_d \approx 1060 \approx z_*$) is given by:

Speed of sound

$$r_{\rm d} = \int_{z_{\rm d}}^{\infty} \frac{c_{\rm s}(z)}{H(z)} dz \qquad c_{\rm s}(z) = \frac{c}{\sqrt{3\left(1+\frac{3\rho_{\rm B}(z)}{4\rho_{\gamma}(z)}\right)}}$$

$$r_{\rm d} = \frac{147.05}{\rm Mpc}\left(\frac{\omega_{\rm m}}{0.1432}\right)^{-0.23}\left(\frac{N_{\rm eff}}{3.04}\right)^{-0.1}\left(\frac{\omega_{\rm b}}{0.02236}\right)^{-0.13}$$

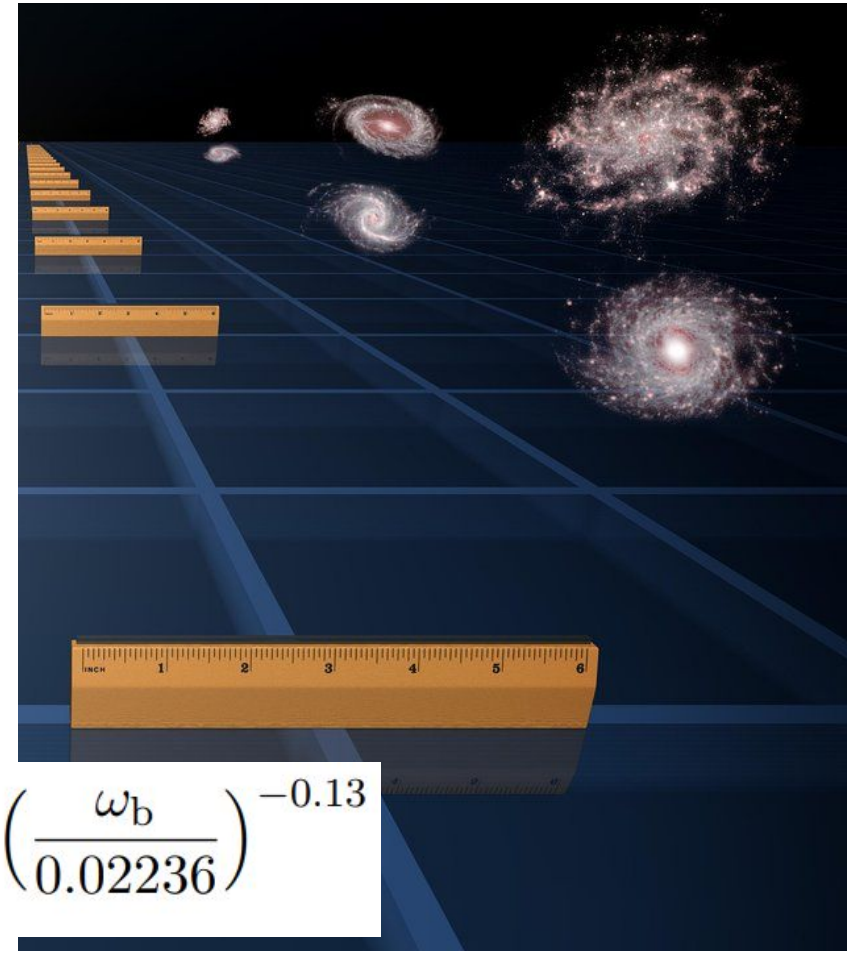

BARYONIC ACOUSTIC OSCILLATIONS

- **Perpendicular to the observer's line-of-sight, a preferred angular separation of galaxies θ can be observed:**

$$\theta = \frac{r_d(z)}{(1+z)d_A(z)}$$

- **Parallel to the observer's line-of-sight, a preferred redshift separation Δz can be observed:**

$$\Delta z = \frac{H(z)r_d}{c}$$

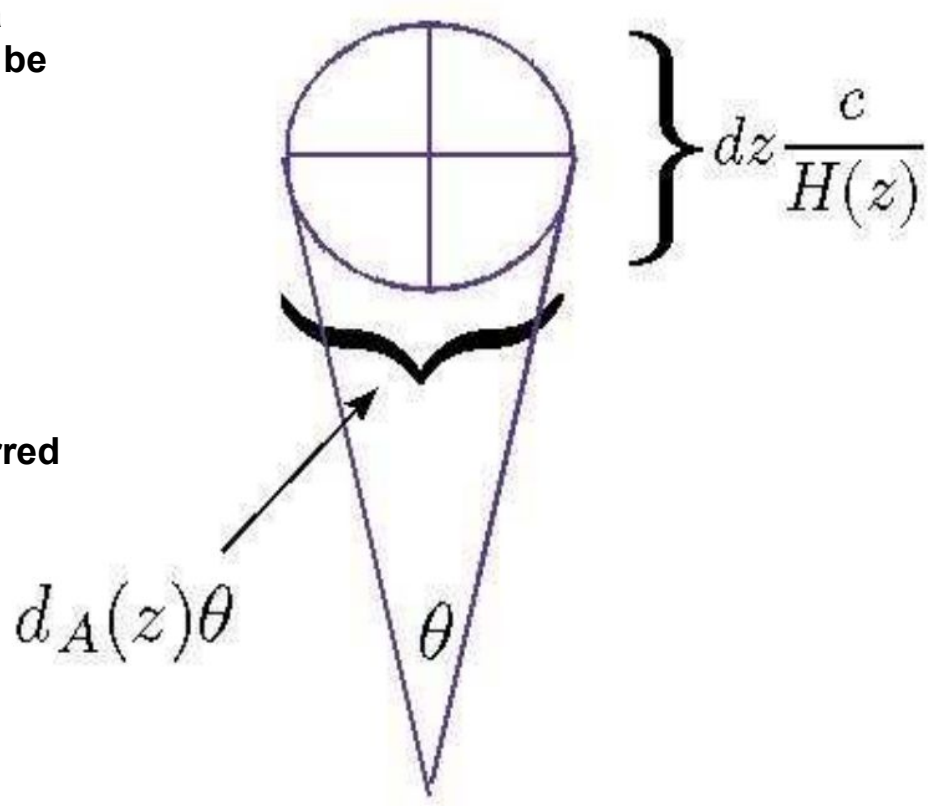

BARYONIC ACOUSTIC OSCILLATIONS

- **For a flat LCDM universe, at late time ($z \ll z_{eq}$):**

Angular diameter distance:

$$d_{\mathrm{A}}(z) = \frac{c}{H_0} \frac{1}{(1+z)} \int_0^z \frac{dz}{\left[\Omega_{\mathrm{m},0}\,(1+z)^3 + \Omega_{\Lambda,0}\right]^{1/2}}$$

Hubble parameter:

$$H(z) = H_0 \sqrt{\Omega_{m,0}(1+z)^3 + \Omega_{\Lambda,0}}$$

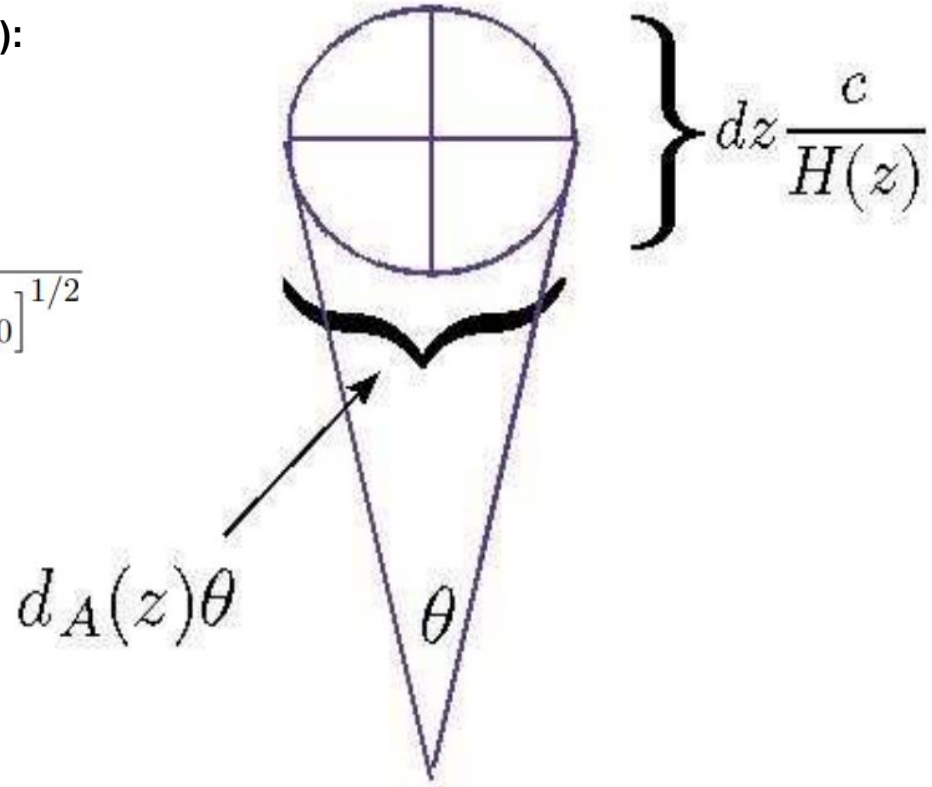

ANGULAR DIAMETER DISTANCE

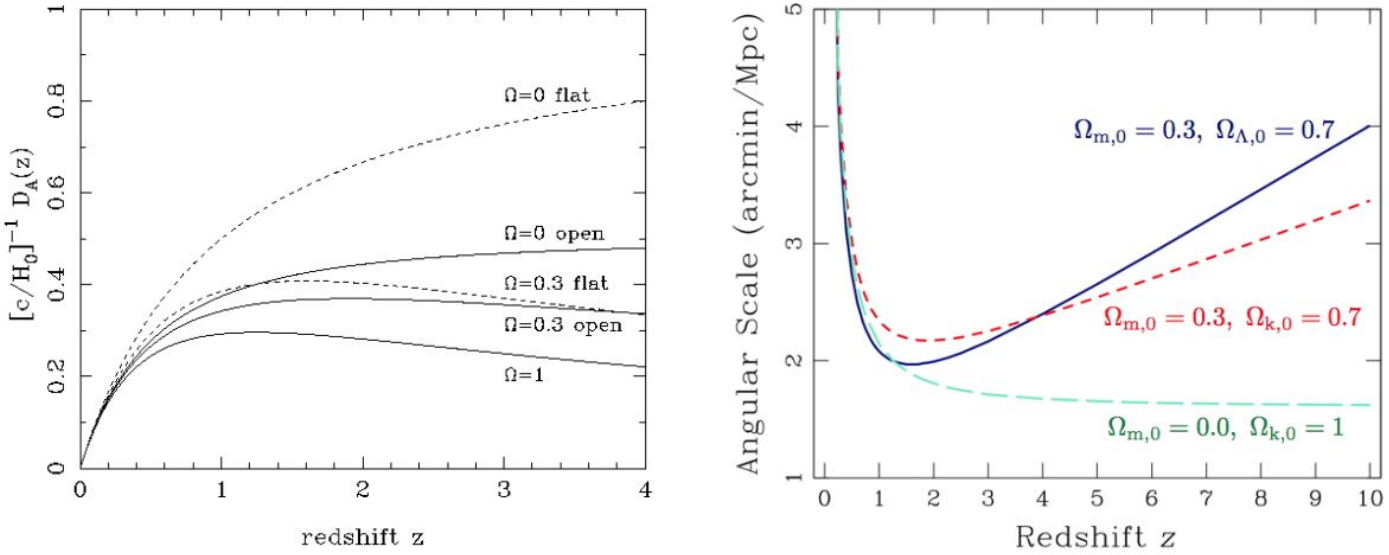

Figure 5.4: *Left:* Plot of the angular diameter distance, $d_{\rm A}$, (in units of c/H_0) as a function of redshift z in different cosmologies (in this figure $\Omega \equiv \Omega_{\rm m,0}$). *Right:* Angle subtended on the sky by an object of proper size $D = 1\,{\rm Mpc}$ as a function of redshift for three different cosmologies, as indicated.

ANGULAR DIAMETER DISTANCE

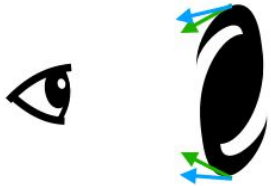

The turnover point occurs because of the expansion of the universe and the finite speed of light: very distant objects were closer to us when they emitted the light we see today. At that time they spanned a larger angle.

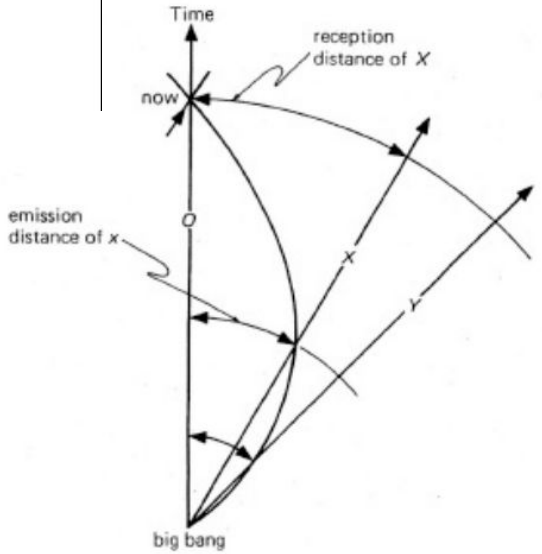

Figure 5.9: O's lightcone curves back into the Big Bang. The diagram shows the reception and emission distances of galaxies X and Y. Although galaxy Y has a greater reception distance, its emission distance is smaller than that of X. Thus Y, which is now further away than X, was closer to us than X at the time of the emission of the light which we now see (reproduced from E. R. Harrison's *Cosmology*).

BAO SCALE FROM GALAXY SURVEY

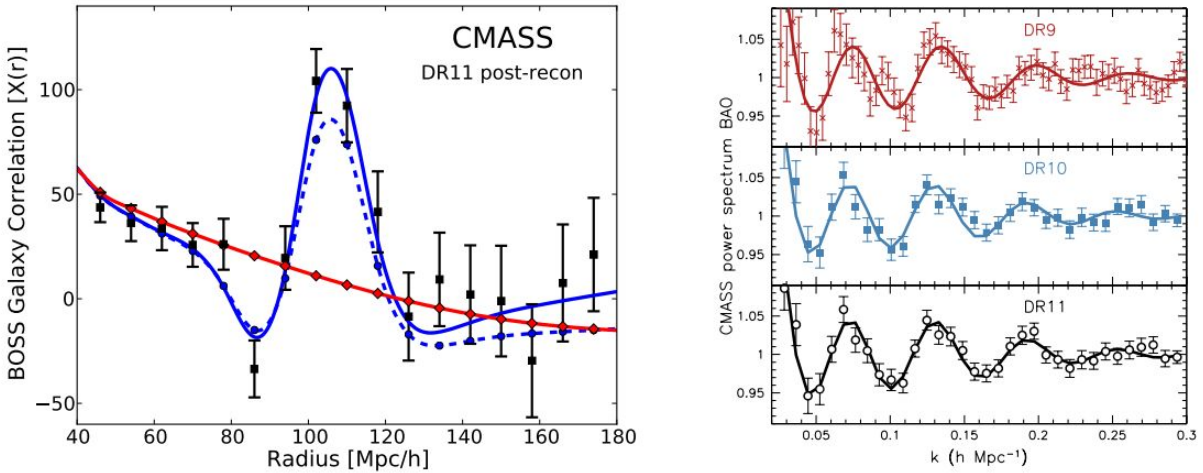

Figure 14.8: *Left:* Baryonic acoustic peak in the two-point correlation function of $\sim 10^6$ galaxies at redshifts $0.4 < z < 0.7$ as determined by the Baryon Oscillation Spectroscopic Survey (BOSS) project. The blue solid line is the best-fit BAO model, while the red line shows the fit by a model which does not include the BAO. *Right:* The BAO feature of the left panel is shown here in the power spectrum of the galaxy distribution: a spike in real space becomes a series of ripples in k-space. The results for three successive data releases of the BOSS project are shown separately. The data and the best fits have been normalised by dividing by the smooth model shown by the red continuous line in the left panel. (Figures reproduced from Anderson et al. 2014).

BAO SCALE FROM GALAXY SURVEY

The inset for each color-coded section of the map includes an image of a typical galaxy or quasar from that section, and also the signal of the pattern that the eBOSS team measures there. As we look out in distance, we look back in time. So, the location of these signals reveals the expansion rate of the Universe at different times in cosmic history.

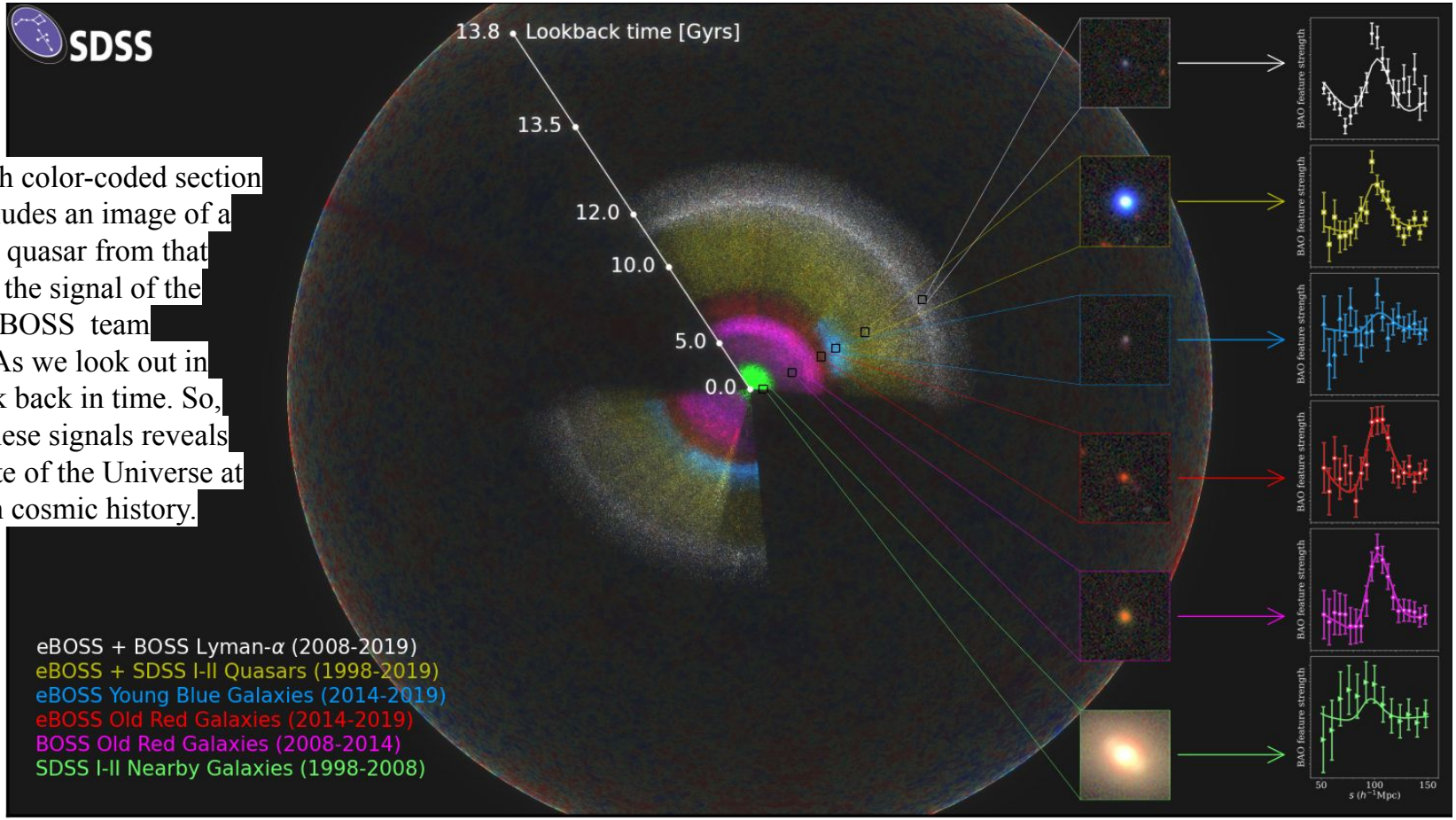

BAO AS STANDARD RULER

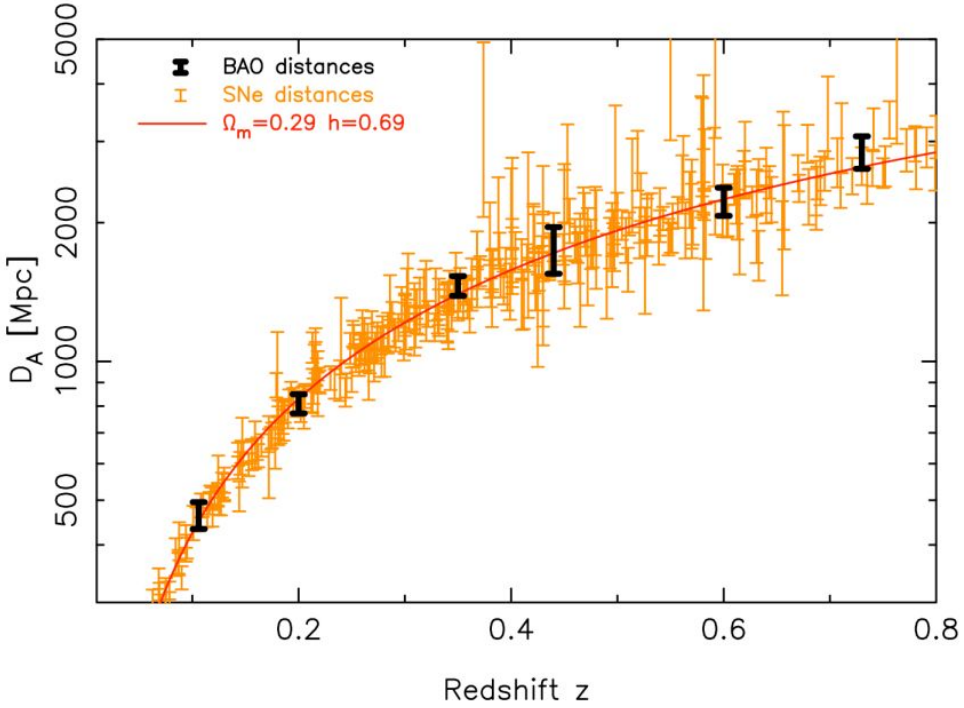

Figure 14.12: Comparison between the SN and BAO mapping of the cosmic distance scale. For the purpose of this figure, the SN $d_{\rm L}$ measurements have been converted to $d_{\rm A}$, assuming $d_{\rm A}(z) = d_{\rm L}(z)/\left(1+z\right)^2$ (Figure reproduced from Blake et al. 2011).

REDSHIFT SPACE DISTORTIONS

Due to peculiar velocities (along the line of sight), the redshift distances available from a galaxy redshift survey deviate from the true, proper distances. This results in redshift space distortions in the clustering measurements.

$$v = v_{\rm exp} + v_{\rm pec} = H_0 d(z) + v_{\rm pec}$$

$$z_{\rm obs} = z_{\rm exp} + \frac{v_{\rm pec}}{c}(1 + z_{\rm exp})$$

L.o.s. Proper Distance measured in redshift space:

$$s = \frac{v}{H_0} = d(z) + \frac{v_{\rm pec}}{H_0}$$

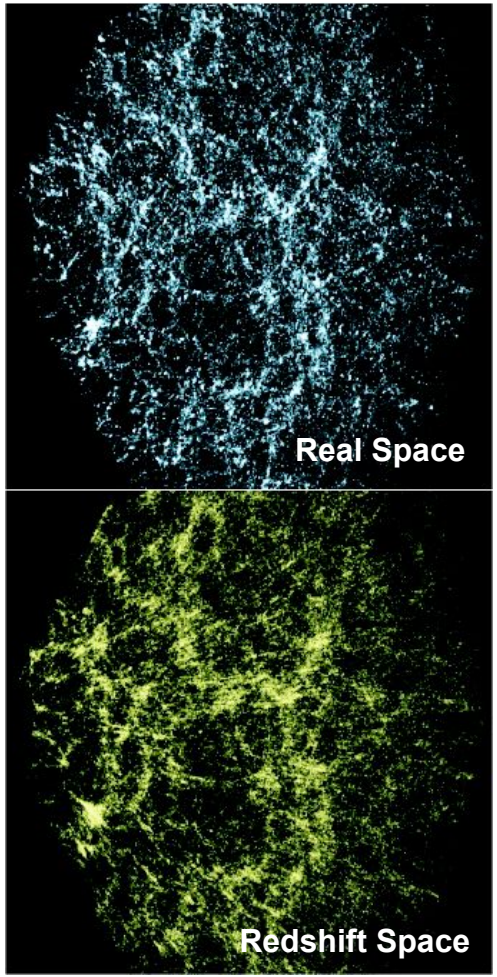

REDSHIFT SPACE DISTORTIONS

- **Kaiser effect:**

On large scales, peculiar velocities reflect the (linear) infall motions towards overdensities, causing a circle in real space to appear "squashed" in redshift space.

- **Finger-of-God effect:**

On small scales, peculiar velocities are due to the nonlinear virialized motion of galaxies inside their host haloes, causing a circle in real space to appear "stretched" in redshift space.

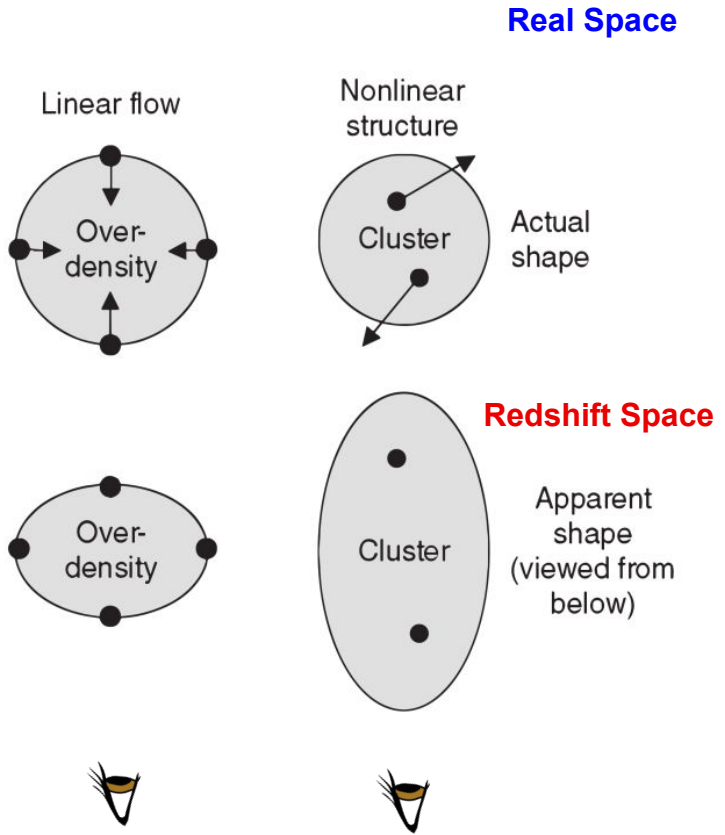

REDSHIFT SPACE DISTORTIONS

Only radial distances are modified by the Doppler effects of peculiar velocities. The complication is that the peculiar velocities arise from the clustering itself. Thus, the apparent clustering pattern in redshift space differs systematically from that in real space and the spatial correlation function of galaxies, which is isotropic in real space is no longer isotropic in redshift space.

We can decompose the distance between two galaxies in their perpendicular and parallel component along the l.o.s.:

$$\pi \equiv \frac{|s \cdot l|}{|l|} \qquad \sigma \equiv \sqrt{s \cdot s - \pi^2}$$

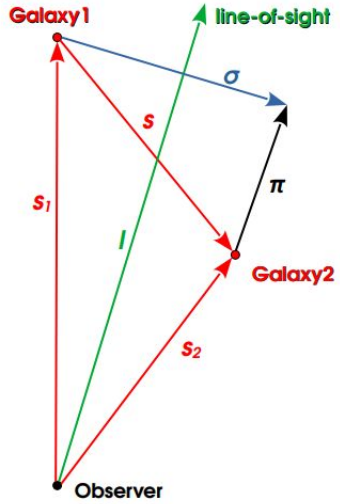

And compute $\xi(\pi, \sigma)$

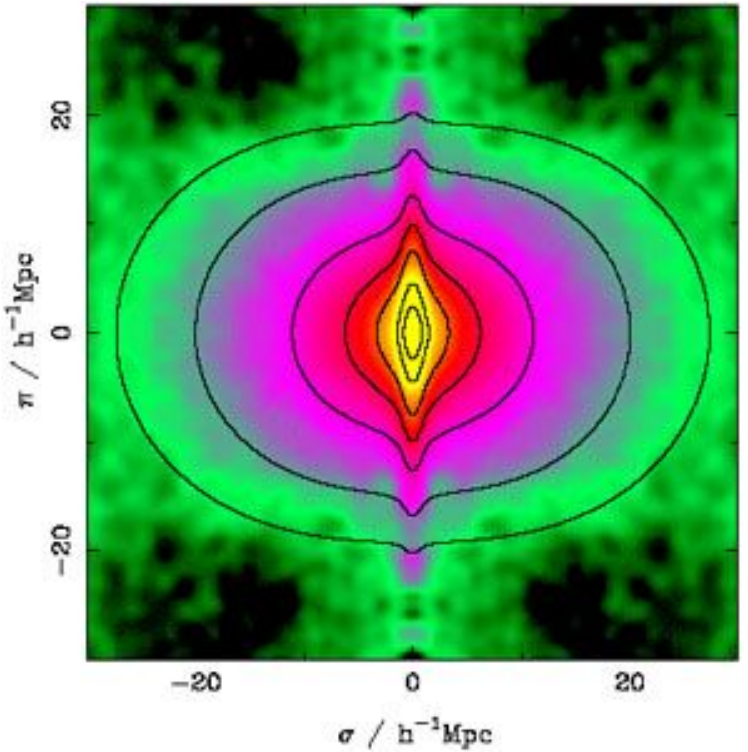

The two-point correlation function obtained from the 2dFGRS by Hawkins et al. (2003). Note the anisotropies due to Finger-of-God and Kaiser effect

REDSHIFT SPACE DISTORTIONS

It can be shown that (in linear theory):

$$\delta_s(\vec{k}) = (1 + \beta\mu^2)\delta_r(\vec{k})$$

$$P_s(k) = (1 + \beta\mu^2)^2 P_r(\vec{k})$$

Where μ is the cosine of the angle between the velocity vector and the line of sight and β is a function of the linear growth rate, *f*, and tracer bias, *b*:

$$\beta = \frac{f(\Omega_m)}{b}$$

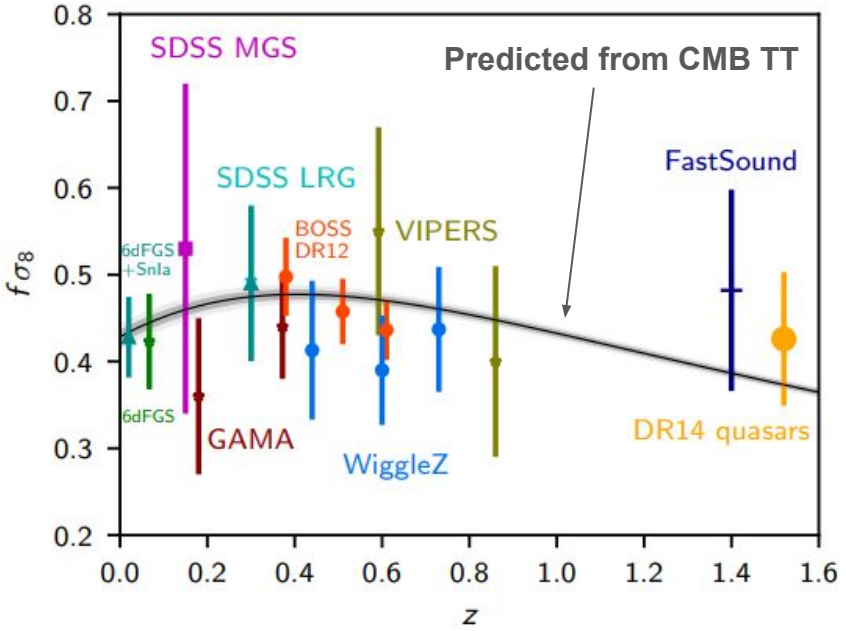

Thus we can use RSD to constrain the growth of structure over cosmic time.

THE KINEMATIC SZ EFFECT

- **The kinematic SZ (kSZ) effect is due to the bulk velocity of the ICM electrons slightly changing the apparent temperature of the CMB black body spectrum.**

- **Amplitude of the pairwise kSZ signal:**

$$T_{\rm pkSZ}(r) \equiv \bar{\tau}_e \frac{v_{12}(r)}{c} T_{\rm CMB}$$

$$v_{12}(r,a) \approx -\frac{2}{3} aH(a) f(a) r \frac{b\bar{\xi}(r)}{1+b^2\xi(r)}$$

ξ(r): Two-point matter correlation function
f(a): Growth rate

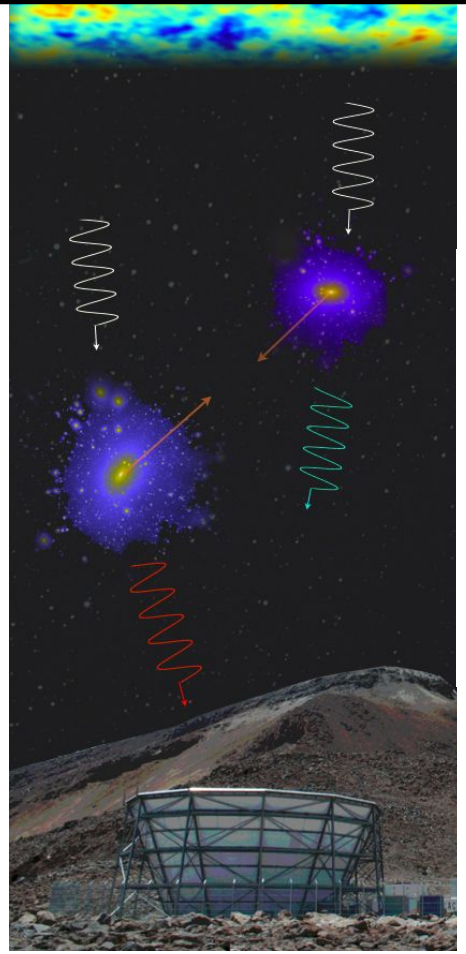

The pkSZ measured from DESI GC and Planck CMB map (Chen+21)

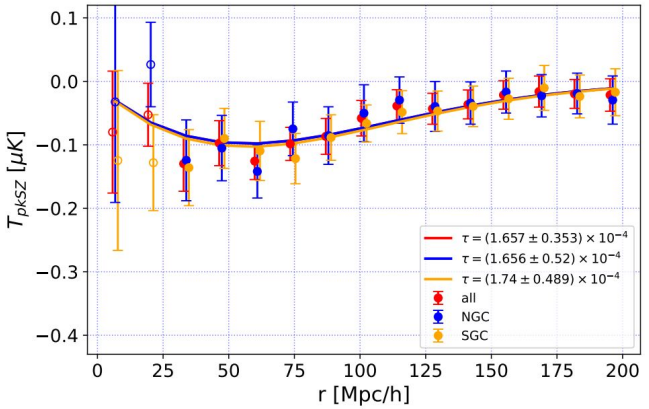

STATISTICAL PROPERTIES OF THE LARGE SCALE STRUCTURES:

COSMIC MICROWAVE BACKGROUND ANISOTROPIES

For a review: https://www.annualreviews.org/content/journals/10.1146/annurev.astro.40.060401.093926
https://ned.ipac.caltech.edu/level5/March05/Scott/Scott_contents.html
https://arxiv.org/pdf/astro-ph/0110414.pdf

COSMIC MICROWAVE BACKGROUND RADIATION

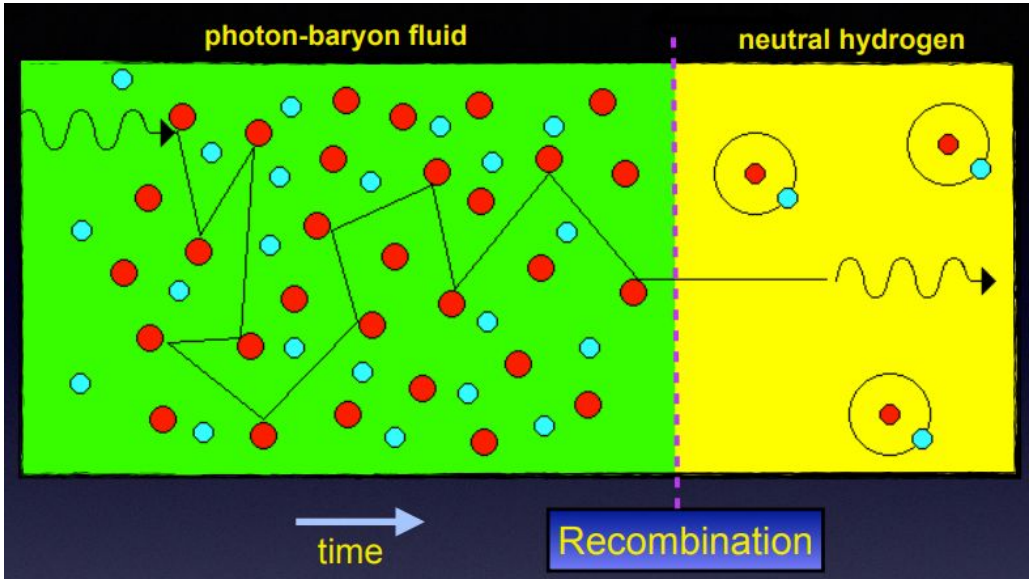

CMB radiation comes to us from last scattering surface (LSS). Since recombination is not instantaneous, in general $z_{LSS} \neq z_{rec}$. Here, the redshift of recombination, is defined as the redshift at which the ionization fraction drops below some value (typically 0.1). Rather $z_{LSS} = z_{dec} \simeq 1100$, where the latter is the redshift of decoupling, defined as the epoch at which the Thomson scattering rate is equal to the Hubble expansion rate

COSMIC MICROWAVE BACKGROUND ANISOTROPIES

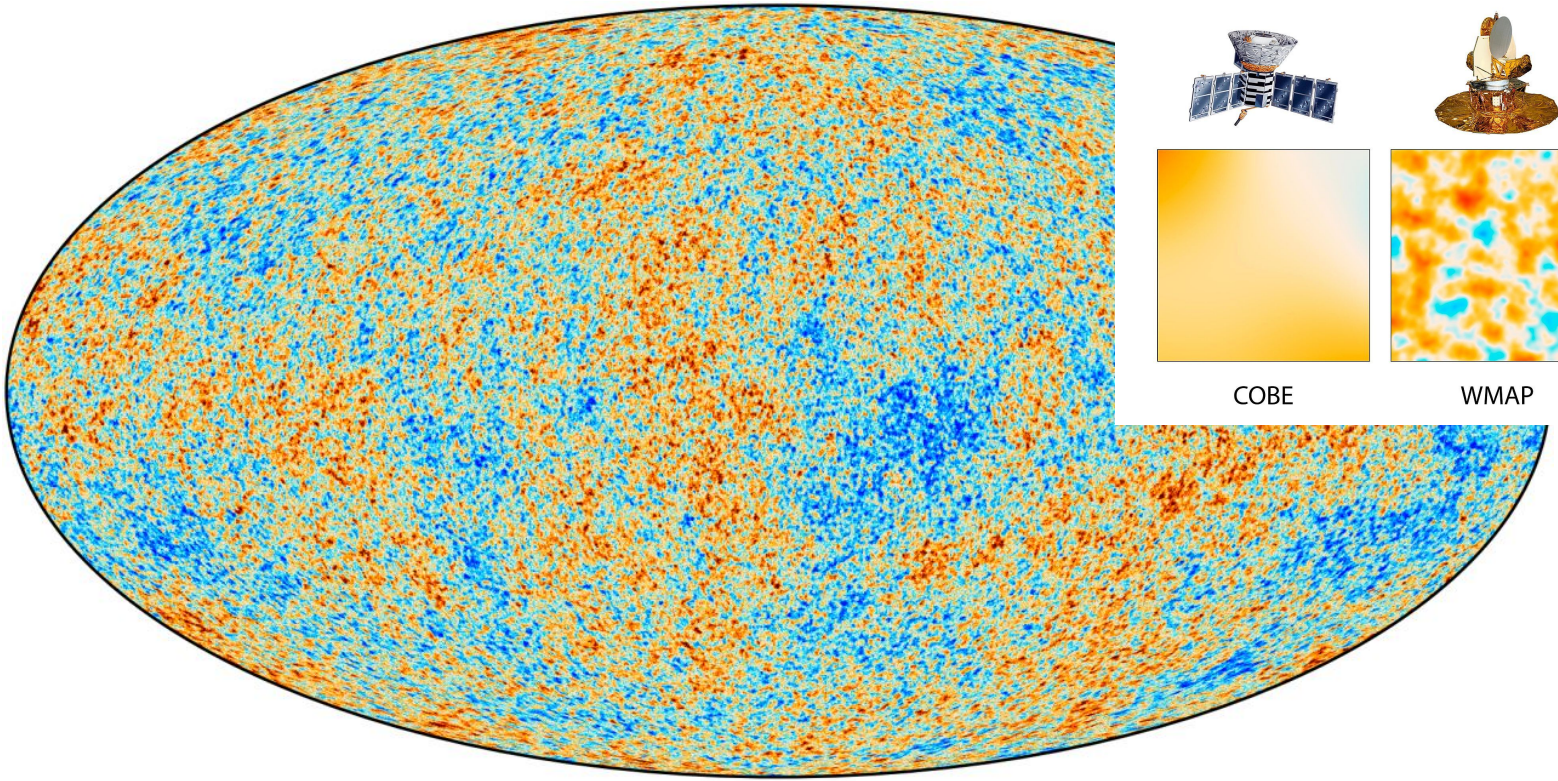

−300 μK 300

THE CMB DIPOLE

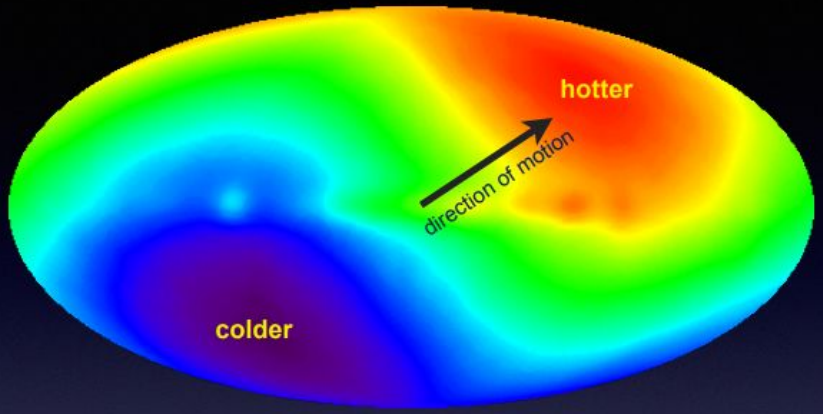

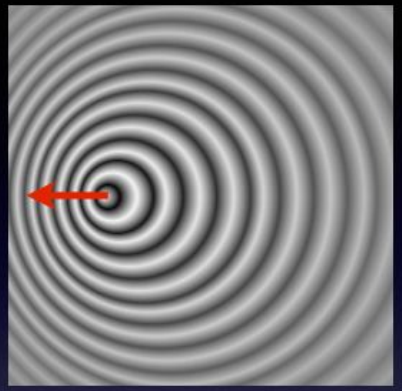

Origin of CMB dipole is Doppler effect due to our peculiar motion

Our peculiar motion is made up of:

- Motion of Earth around Sun (~30 km/s)
- Motion of Sun around MW center (~220 km/s)
- Motion of MW towards Virgo cluster (~300 km/s)

Total vector sum of 369 km/s

Photons coming from the direction in which we are moving are blueshifted (as if that direction is moving towards us). Photons of a shorter wavelength correspond to photons of a higher temperature (i.e., Wien's law)

COSMIC MICROWAVE BACKGROUND ANISOTROPIES

Define the CMB anisotropy distribution

$$\Theta(\hat{n}) \equiv \frac{\Delta T}{T}(\hat{n}) = \frac{T(\hat{n}) - \bar{T}}{\bar{T}}$$

Here $\hat{n} = (\vartheta, \phi)$ is direction on the sky, and $\bar{T}$ is the average CMB temperature.

We expand this in Spherical Harmonics:

$$\Theta(\hat{n}) = \sum_{l,m} a_{lm}\, Y_{lm}(\vartheta, \phi)$$

and define the power spectrum as

$$\mathcal{C}_l = \langle |a_{lm}|^2 \rangle$$

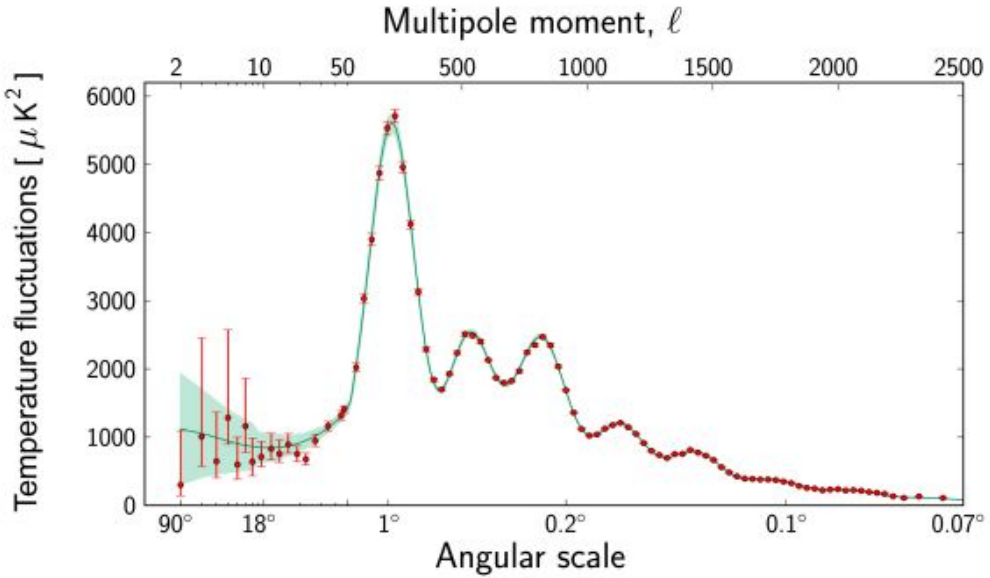

COSMIC MICROWAVE BACKGROUND ANISOTROPIES

An important angular scale is that corresponding to the comoving Hubble radius at decoupling, $r_H = c/H(z_{dec})$:

$$\theta_H = \frac{r_H}{d_A(z_{\rm dec})(1+z_{\rm dec})} \simeq 0.87^\circ$$

Which corresponds to $\ell \simeq 200$; CMB anisotropies with $\ell < 200$ correspond to super-horizon scale perturbations. On these super-horizon scales, only two effects can contribute to non-zero $\Delta T / T$ fluctuations:

i) fluctuations of the photon density at decoupling
ii) fluctuations in the gravitational potential (photons lose energy when climbing out of a potential well)

The combination of these two effects is known as the Sachs-Wolfe effect

The relation between ℓ and the associated angular scale ϑ is: $\theta \sim \frac{\pi}{\ell}\text{rad} \sim \frac{180^\circ}{\ell}$

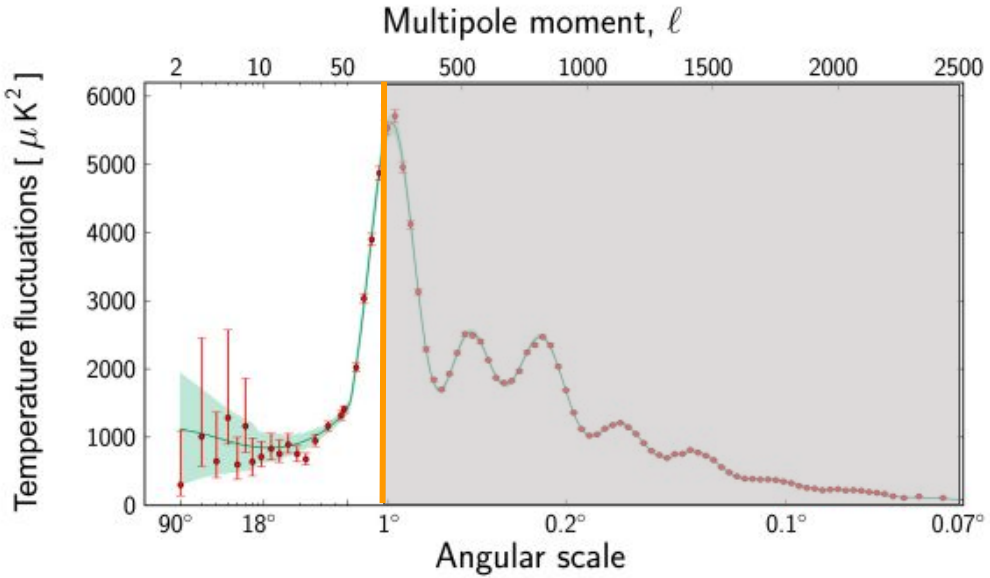

CMB ACOUSTIC PEAKS

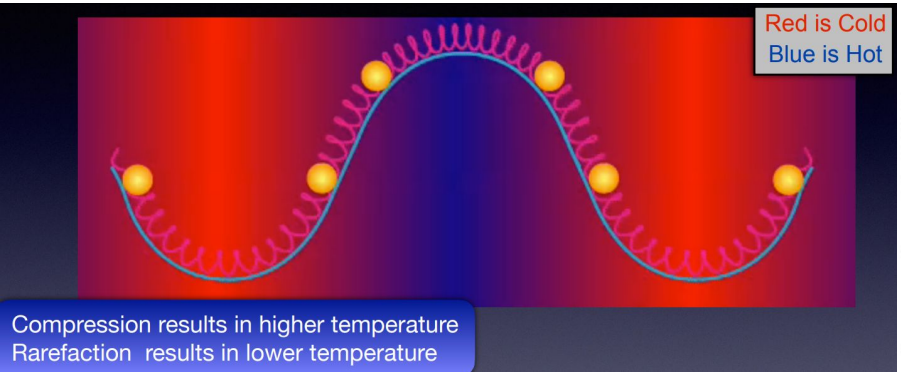

On sub-horizon scales the rich structure observed in the temperature anisotropy spectrum is mainly a consequence of the acoustic oscillations of the tightly-coupled baryon-photon fluid in the pre-recombination era. Perturbations in the gravitational potential, dominated by the CDM component, drive the oscillations in the plasma, with photon pressure, due to Thomson scattering of photons off free electrons, providing most of the restoring force.

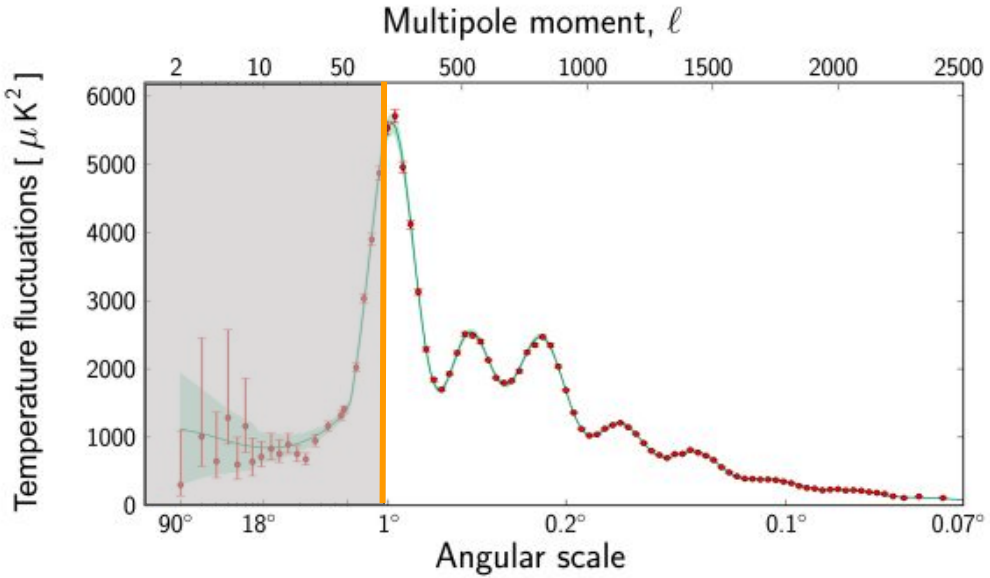

After recombination, photons can travel freely toward us, and the phases of the oscillations is imprinted in the CMB spectrum as a series of harmonic peaks. The last-scattering surface is a snapshot view of oscillation phases of all different modes.

CMB ACOUSTIC PEAKS

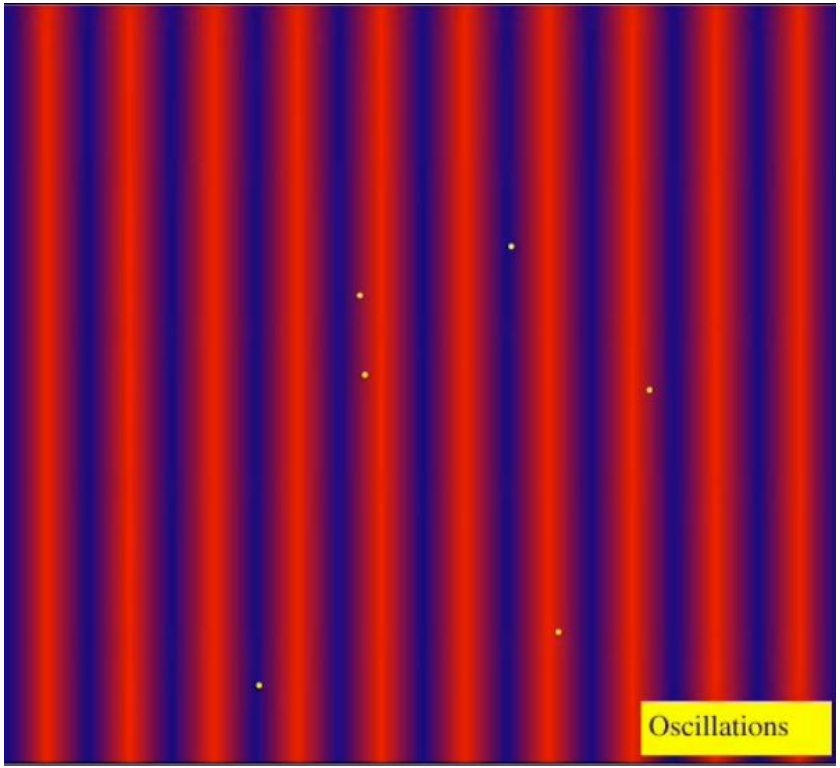

If we consider a single perturbation mode

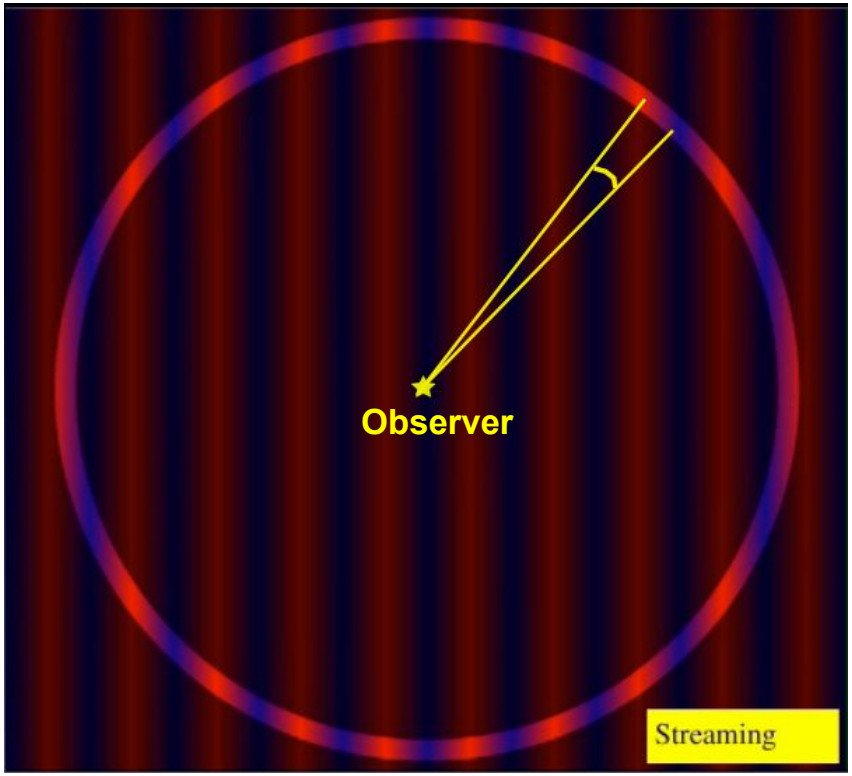

The observer sees this mode as angular temperature fluctuation on the sky, with a characteristic angular scale set by the wavelength of the mode

CMB ACOUSTIC PEAKS

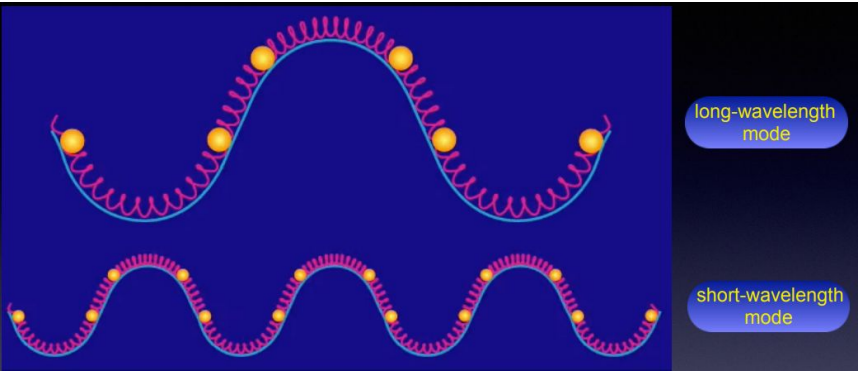

Since sound speed of photon-baryon fluid is the same for all modes, those with a smaller wavelengths oscillate faster.

The first peak corresponds to the mode that is caught in its first compression by recombination. The second peak corresponds to the mode that went through a full cycle of compression and rarefaction by recombination. The even peaks are generally of smaller amplitude because the rebound has to fight against baryon inertia.

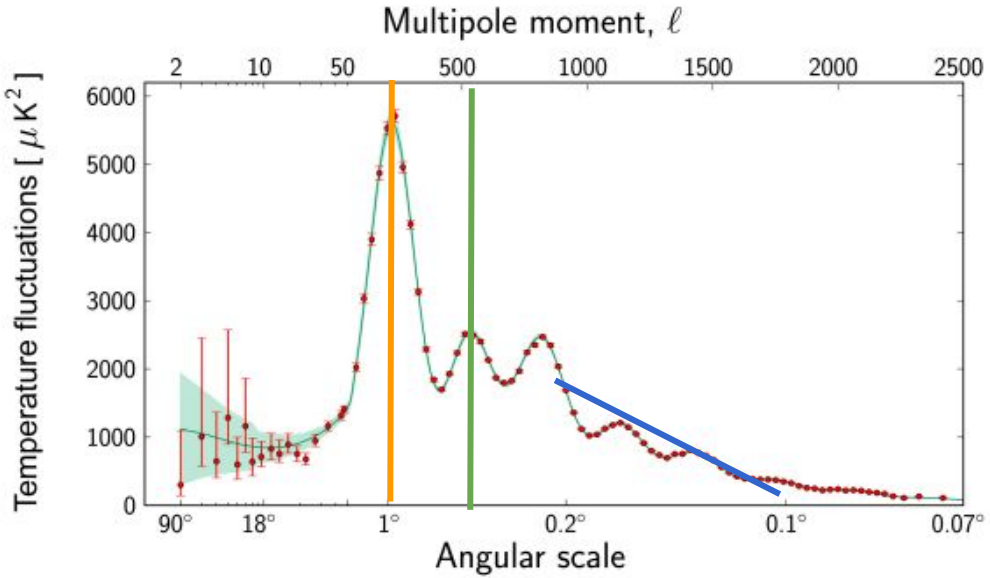

Since the recombination process is not instantaneous, the last scattering surface has a finite thickness. This leads to a smearing of the anisotropies on scales smaller than the width ($\Delta z \simeq 80$) of the recombination process, $\ell > 1000$ (diffusion damping)

CMB SECONDARY ANISOTROPIES

At angular scales smaller than few arc-minutes CMB temperature fluctuations are no longer dominated by primary effects at the surface of last scattering, but rather by the so-called secondary anisotropies which arise from the interaction of the CMB photons with the matter along the line of sight. The secondary anisotropies can be divided in two major families depending on the physical process which generate them. The first family arises from the interaction of the photons with gravitational potential wells, and it includes gravitational lensing and the late ISW effect. As for former, the gravitational deflection of CMB photons by intertwining non-linear structures causes a smoothing of the acoustic peaks up to 10% level at $\ell > 2000$, and generate small-scale power that dominates the primary anisotropies for $\ell > 4000$, where the diffusion damping is highly effective. Moreover, CMB lensing introduces non-Gaussianity in the four-point correlation function with a very specific and predictable shape, from which it is possible to reconstruct the power spectrum of the lensing potential. The second family incorporates the effects of scattering of CMB photons with free electrons, such as reionization effects and the Sunyaev and Zeldovich effect (see previous lectures).

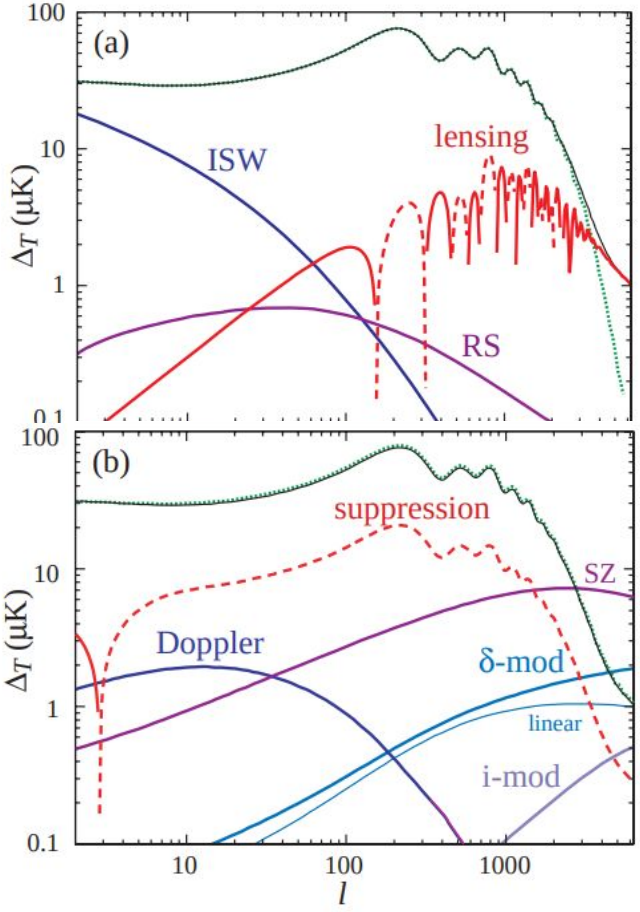

Credit: Hu & Dodelson 2002

CMB TEMPERATURE POWER SPECTRUM

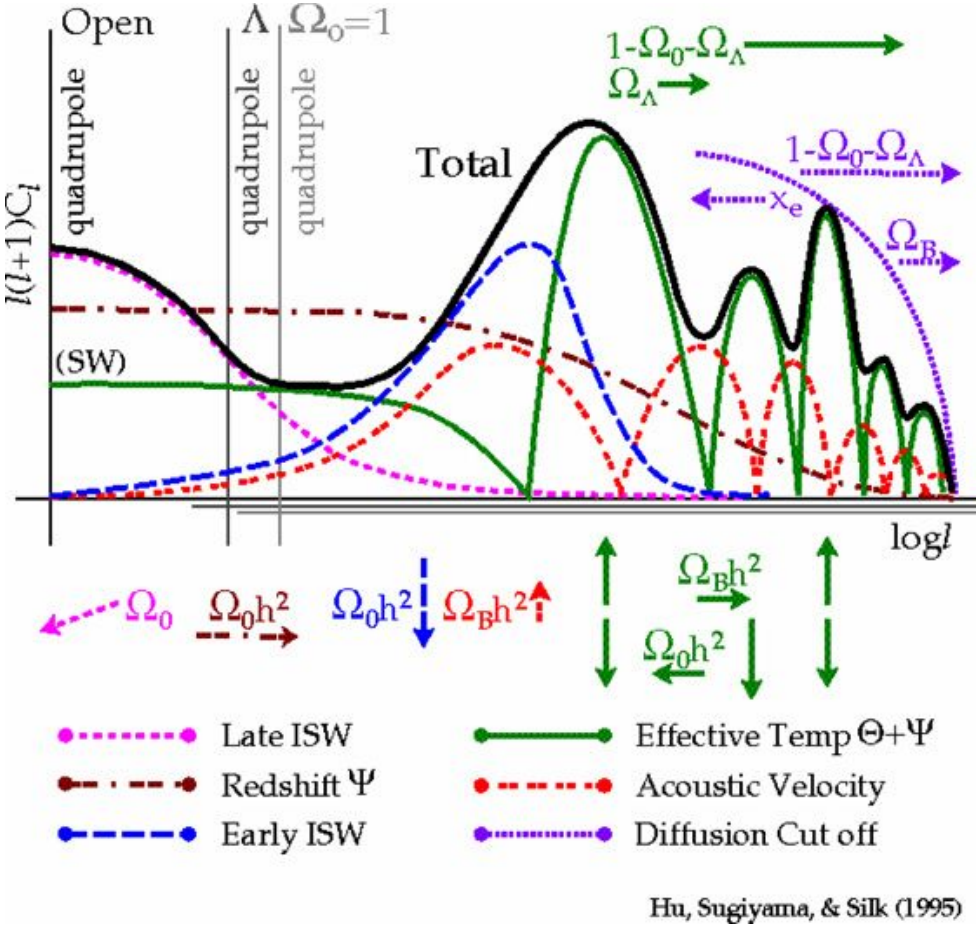

Contributions to the CMB temperature power spectrum of various physical processes and their dependence on Ω_m , Ω_b , Ω_Λ . Features in open models ($\Omega_k = 1 - \Omega_m - \Omega_\Lambda > 0$) are shifted to larger *l* compared to flat ΛCDM (Λ) or EdS ($\Omega_m = 1$) models, represented here as a shift of the origin of the x-axis (ℓ=2 quadrupole). Contributions from different physical processes are shown with different line styles (see legend). The arrows indicate the direction of change of the various contribution led by the increase of the model parameter written aside. For example, an increase of $\Omega_b h^2$ increases the heights of the first and third acoustic peaks, shifts the peaks to larger *l* and increases the overall contribution of the acoustic velocity peaks.

CMB TEMPERATURE POWER SPECTRUM

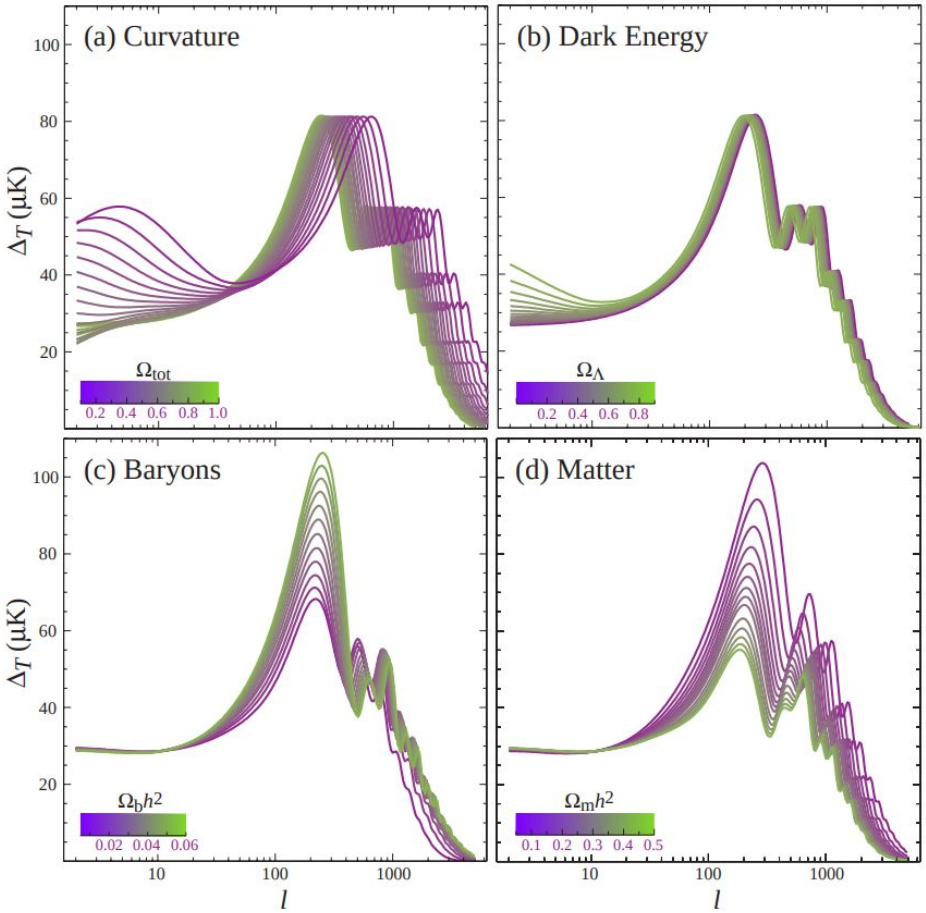

Credit: Hu & Dodelson 2002

The position of the acoustic peaks are determined by the physical size of the sound horizon at decoupling, and the angular diameter distance of the last scattering surface. Thus, the position of the peaks depends on the geometry of the space and on the value of Ω_b. Furthermore, the value of Ω_b controls also the relative amplitude between even and odd peaks and the depth of the valleys. In addition, the heights of the acoustic peaks can be affected by the strength of the initial perturbations (A_s and n_s) , and by Ω_m through to the time evolution of the gravitational potential induced by the self-gravity of the acoustic perturbations.

CMB POLARIZATION POWER SPECTRUM

Thomson scattering of a radiation field with a quadrupole anisotropy produces linear polarization. The relevant epoch for the generation of polarization in the CMB is around recombination since at early times scattering is too efficient to allow a significant quadrupole to grow, while after recombination scatterings are very rare (until the universe reionizes).

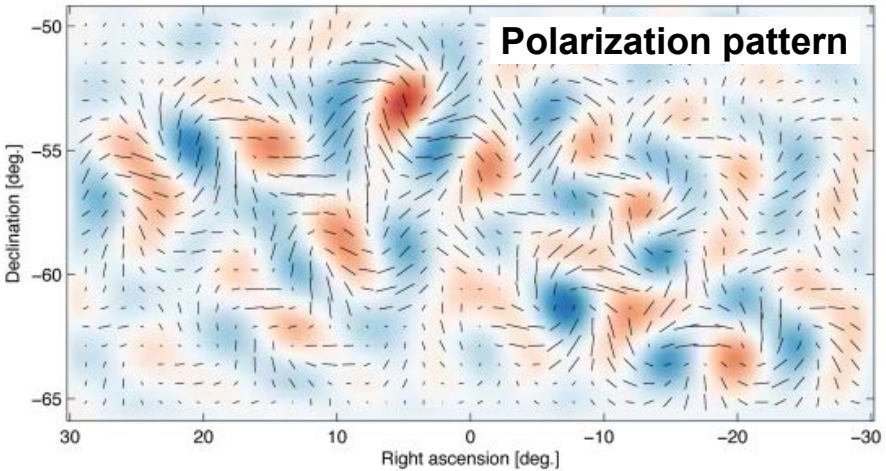

From acoustic density perturbations

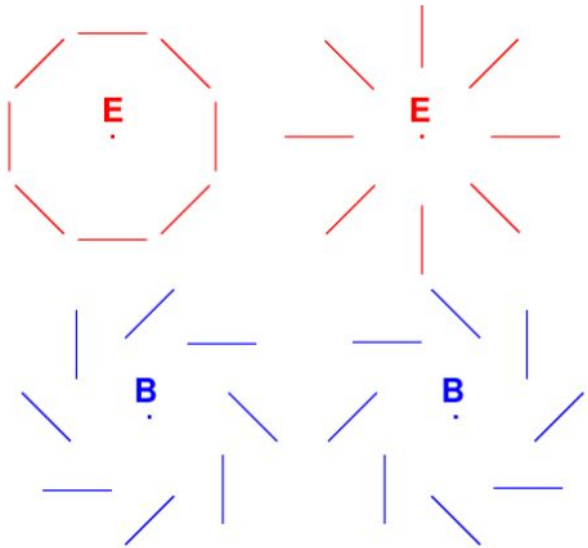

From primordial gravitational waves or lensing

CMB POLARIZATION POWER SPECTRUM

The CMB polarization signal is expected to have a r.m.s. of ~ 5μK, peaking at multipoles l ≃ 1000 (the angle subtended by the photon mean free path at last scattering). The amplitude of the polarization signal is much smaller than the temperature power spectrum.

B-mode polarization can be induced by tensor perturbation, generated by the primordial gravitational waves predicted in the inflationary scenario, or by gravitational lensing due to the intertwining structures along the line of sight. A measurement of the gravitational waves power probes directly the energy scale of inflation.

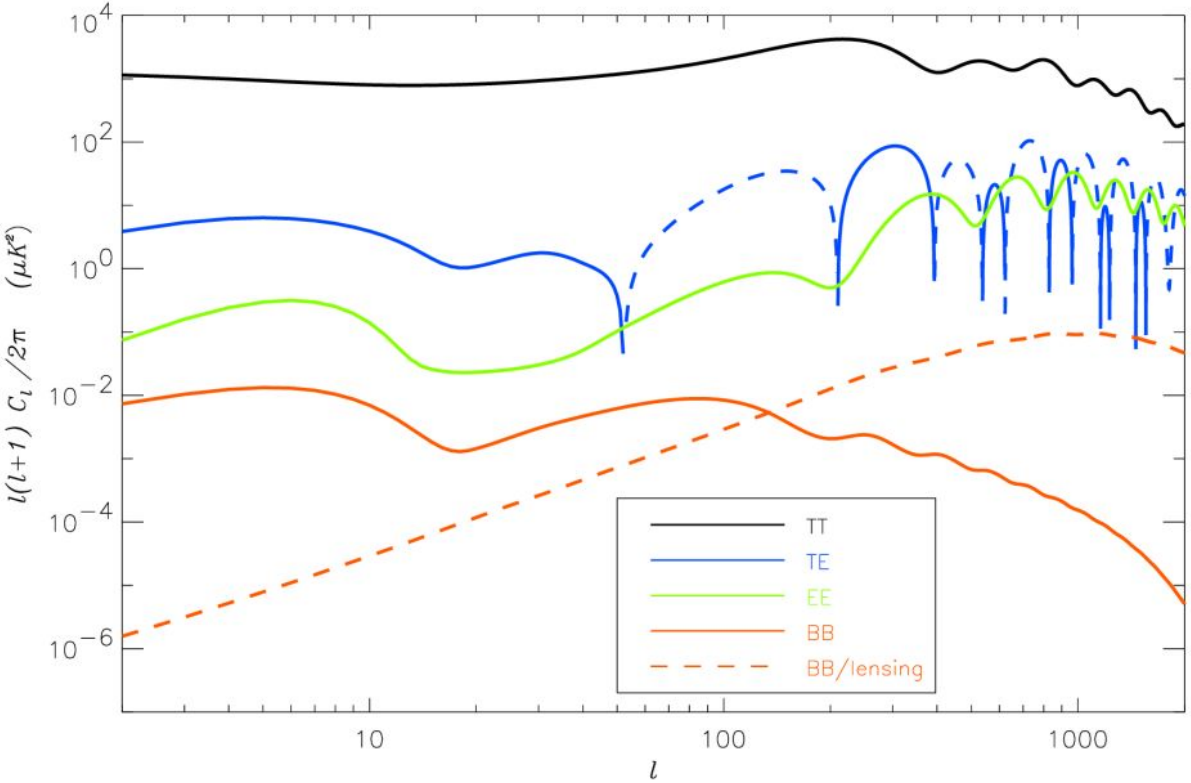

The ”bump” at low multipoles (l< 20) in the polarization spectra is due to the re-scattering of CMB photons at reionization. The position of this peak is set by the size of the horizon at reionisation, while its amplitude is determined by the duration of the ionization process.

CONSTRAINTS FROM CMB DATA

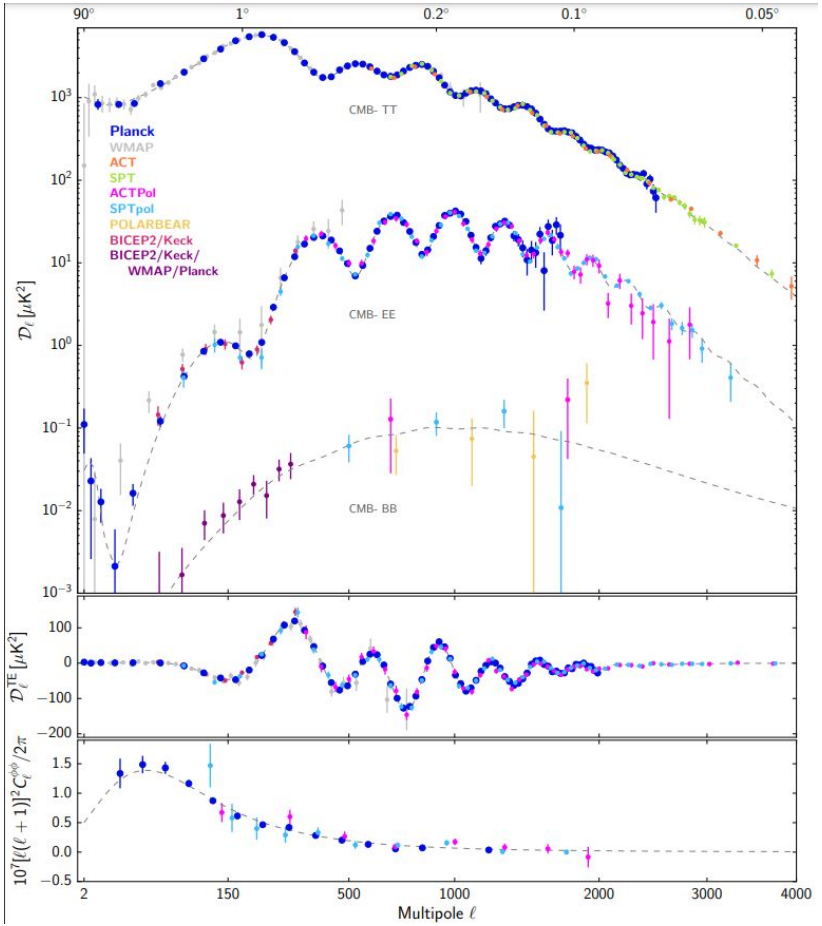

Nowadays CMB data (temperature and polarization) provides the single-probe tighter constraints on the ΛCDM model parameters.
All sky surveys, like Planck, are cosmic variance limited (especially at the largest scale, low ℓ).
Combining CMB experiments with different angular resolution and sky coverage allow to improve the constraining power by increasing the multipole range that can be probed (e.g. Planck and SPT)

	SPT-3G 2018	SPT-3G 2018 + *Planck*
$\Omega_b h^2$	0.02224 ± 0.00032	0.02233 ± 0.00013
$\Omega_c h^2$	0.1166 ± 0.0038	0.1201 ± 0.0012
$100\theta_{MC}$	1.04025 ± 0.00074	1.04075 ± 0.00028
$10^9 A_s e^{-2\tau}$	1.871 ± 0.030	1.884 ± 0.010
n_s	0.970 ± 0.016	0.9649 ± 0.0041
$H_0\ [\mathrm{km\,s^{-1}\,Mpc^{-1}}]$	68.3 ± 1.5	67.24 ± 0.54
σ_8	0.797 ± 0.015	0.8099 ± 0.0067
$S_8 \equiv \sigma_8 \sqrt{\Omega_m/0.3}$	0.797 ± 0.042	0.832 ± 0.014
Ω_Λ	0.700 ± 0.021	0.6835 ± 0.0075
Age/Gyr	13.815 ± 0.047	13.807 ± 0.021

CONSTRAINTS FROM CMB DATA

https://arxiv.org/pdf/2212.05642.pdf

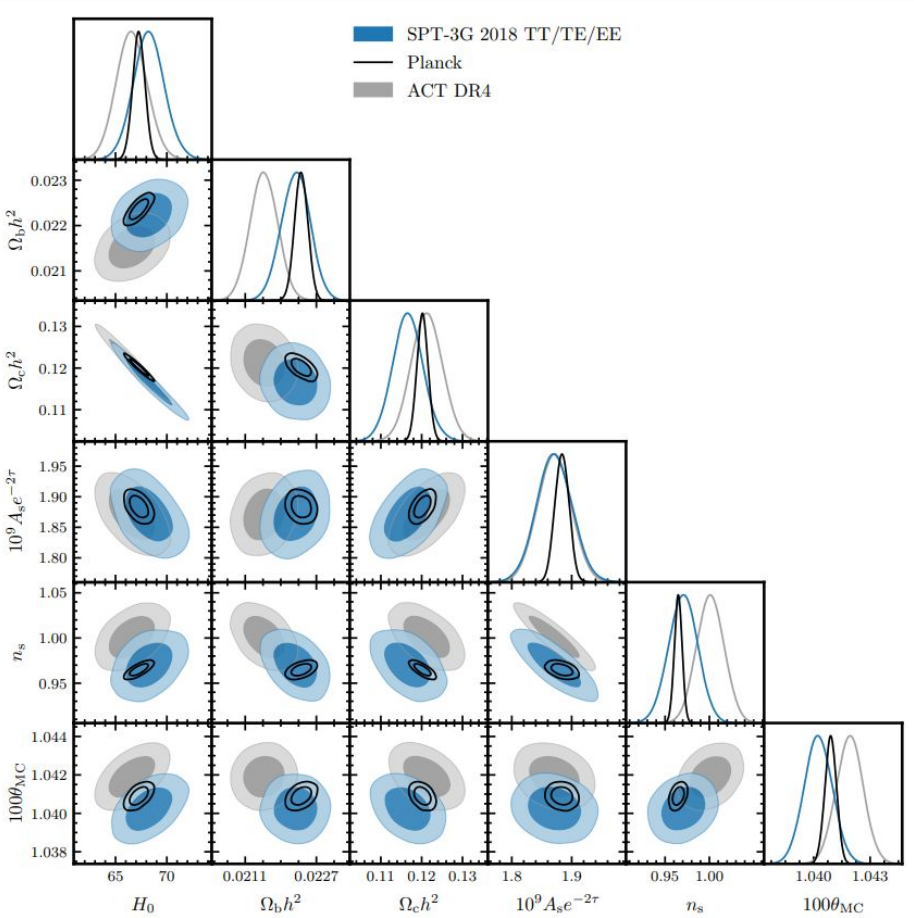

Nowadays CMB data (temperature and polarization) provides the single-probe tighter constraints on the ΛCDM model parameters.
All sky surveys, like Planck, are cosmic variance limited (especially at the largest scale, low ℓ).
Combining CMB experiments with different angular resolution and sky coverage allow to improve the constraining power by increasing the multipole range that can be probed (e.g. Planck and SPT)

	SPT-3G 2018	SPT-3G 2018 + *Planck*
$\Omega_b h^2$	0.02224 ± 0.00032	0.02233 ± 0.00013
$\Omega_c h^2$	0.1166 ± 0.0038	0.1201 ± 0.0012
$100\theta_{MC}$	1.04025 ± 0.00074	1.04075 ± 0.00028
$10^9 A_s e^{-2\tau}$	1.871 ± 0.030	1.884 ± 0.010
n_s	0.970 ± 0.016	0.9649 ± 0.0041
H_0 [km s^{-1} Mpc^{-1}]	68.3 ± 1.5	67.24 ± 0.54
σ_8	0.797 ± 0.015	0.8099 ± 0.0067
$S_8 \equiv \sigma_8 \sqrt{\Omega_m/0.3}$	0.797 ± 0.042	0.832 ± 0.014
Ω_Λ	0.700 ± 0.021	0.6835 ± 0.0075
Age/Gyr	13.815 ± 0.047	13.807 ± 0.021